Laser and Particle Beams (2001), *19*, 631–642. Printed in the USA.

DOI: 10.1017.S0263034601194103

A cellular automaton model of laser–plasma interactions

DIMITRI BATANI,[1] SABRINA BIAVA,[2] SERGIO BITTANTI,[2] AND FABIO PREVIDI[2]

[1]Dipartimento di Fisica "G. Occhialini," Università di Milano-Bicocca, INFM, Unità di Milano-Bicocca, Piazza della Scienza 3, 20126 Milano, Italy
[2]Dipartimento di Ingegneria, Universita' di Bergamo, Via Marconi 5, 24044 Dalmine (Bg), Italy

(RECEIVED 1 June 2000; ACCEPTED 11 June 2001)

Abstract

This paper deals with the realization of a CA model of the physical interactions occurring when high-power laser pulses are focused on plasma targets. The low-level and microscopic physical laws of interactions among the plasma and the photons in the pulse are described. In particular, electron–electron interaction via the Coulomb force and photon–electron interaction due to ponderomotive forces are considered. Moreover, the dependence on time and space of the index of refraction is taken into account, as a consequence of electron motion in the plasma. Ions are considered as a fixed background. Simulations of these interactions are provided in different conditions and the macroscopic dynamics of the system, in agreement with the experimental behavior, are evidenced.

Keywords: Cellular automata; Laser-plasma interaction; Physical-based modeling

1. INTRODUCTION

The recent advent of femtosecond lasers (Mourou *et al.*, 1998; Nisoli *et al.*, 1998) has opened new perspectives in the research on laser-produced plasmas. In particular, important new results have been obtained in the field of soft X-ray lasers (Zepf *et al.*, 1998b); high order harmonics generation and its applications (Zepf *et al.*, 1998a); sources of relativistic particles (Key, 1999); laser acceleration of electrons (Modena *et al.*, 1995; Dalla & Lontano, 1995); highly nonlinear interactions and laser beam self-focusing (Amiranoff *et al.*, 1995; Lontano, 1995); and the new "fast ignitor" approach to inertial confinement fusion, ICF (Tabak *et al.*, 1994; Atzeni, 1995), including in particular the generation of fast electrons and their propagation in dense matter (Hall *et al.*, 1998; Bernardinello *et al.*, 1999; Gremillet *et al.*, 1999; Batani *et al.*, 2000; Pisani *et al.*, 2000).

Sophisticated computer codes are already available to simulate plasmas produced by such short laser pulses, including particle-in-cell (PIC) codes (Pukhov & Meyer-ter-Vehn, 1998), Vlasov codes (Macchi *et al.*, 1998; Ruhl *et al.*, 1998) and Fokker–Planck codes (Davies *et al.*, 1997).

In this paper, a cellular automaton (CA) model of laser–plasma interaction will be presented. In particular, the interaction between a short laser pulse and a fully ionized plasma will be considered. The development of simulation tools based on cellular automata appears very interesting for a number of reasons. First of all, CA codes allow a direct representation of low-level elementary physical laws, the complex macroscopic dynamics of the global system emerging from "simple" microscopic interaction rules among the cells of the CA. In some situations, this may allow a better or simpler understanding on the ongoing physics (see, e.g., Wolfram, 1983; Toffoli, 1984; Bennet *et al.*, 1986; Frish *et al.*, 1986; Dab & Boon, 1990; Bruschi *et al.*, 1992; Cattaneo *et al.*, 1996). In general, the goal of all computer codes is to describe complex phenomena starting from simpler ones. This is particularly true for CA models. Here the "low-level" description may be particularly "simple" because everything in CA models is treated through "forces" acting between cells (particles).

Moreover, usually in the experimental protocols, the laser generates very short pulses (≈100 fs) which are focused on a small focal spot ($d \approx 10$ μm) to obtain the high intensity necessary to create and study the plasma. The transversal dimension of the region filled with the plasma is of the order of the focal spot size; the longitudinal dimension is of the order of the focal depth of the lens ($L \approx 100$ μm). So, the physical phenomena that are the subject of the simulation are confined in a very small region of space and take place in a very short time. Thus, it is possible to conceive a CA code that performs a 1:1 simulation of the laser–plasma inter-

Address correspondence and reprint request to: Dimitri Batani, Dipartimento di Fisica "G. Occhialini," Università di Milano-Bicocca, INFM, Unità di Milano-Bicocca, Piazza della Scienza 3, 20126 Milano, Italy. E-mail: batani@mib.infn.it

action dynamics. In other words, CA could allow the simulation of the "true" dynamical evolution of the system with a very high temporal and spatial resolution.

Basically, CA may be used in two different ways: as computational tools, for solving differential equations, used together with parallel computers (Doolen, 1991), or as a dynamical systems completely discrete (both in time and state variables) used as a physical-based model (Toffoli, 1984; Cattaneo *et al.*, 1996; Previdi & Milani, 1998; Previdi, 2000). In this work, the second approach is followed, using a cellular automaton to describe the radiation-matter interaction between a laser pulse and a hot plasma.

CA have already been used for direct physical-based modeling of systems. In particular, applications can be found in biology for DNA sequences modeling (Burks & Farmer, 1984) and cytoskeleton formation modeling (Smith *et al.*, 1984); in vulcanology to simulate lava streams (Di Gregorio *et al.*, 1996); for bioremediation of contaminated soils (Spezzano & Talia, 1998); in hydrodynamics, for turbulence simulation (Frish *et al.*, 1986); in chemistry, for the investigation of crystal growth dynamics (Packard, 1985); in optoelectronics, for simulation of the behavior of semiconductor-integrated optical devices (Cattaneo *et al.*, 1996; Previdi & Milani, 1998).

In plasma physics, in the past, CA models have already been used to simulate other aspects of plasma physics, in particular the plasma hydrodynamical behavior (Chen *et al.*, 1988a, 1988b). The objective of the paper is to see to what extent laser–plasma interaction can be described by using a CA model. Hence here we rather focus on aspects which were not treated in previous works, that is, to the plasma–radiation interaction. Although this is a preliminary work, it shows some possibilities, but also the main difficulties related to the use of CA for the simulation of laser–plasma interactions.

The paper has the following structure: in Section 2, a presentation is given of the CA as discrete (in time and state variables) dynamical systems. In Section 3, the basic physical laws of laser–plasma interaction are introduced. Section 4 is devoted to the outline of the CA implementation of the physics described in the previous section. Section 5 contains the simulation results presented following a step-by-step procedure, that is, by separately presenting the effects of each single interaction and, finally, by merging all the rules of evolution in a single CA model.

2. CELLULAR AUTOMATA AS A DISCRETE-EVENT DYNAMICAL SYSTEMS

Cellular automata are discrete time dynamical systems made by many identical and simple interconnected subsystems, called *cells*. Each cell interacts with a finite number of other cells, that is, those belonging to a user-defined *neighborhood*. The interaction among each cell and its neighborhood is governed by suitable set of *rules of evolution*. A number of *state variables* can be defined as function of space (through the cell position in the CA) and time. So, a CA model is fully defined by the following items:

- the *cellular space*, which is a discrete lattice of spatially distributed cells;
- the *state variables* defined for each cell;
- the *neighborhood of a cell*, **N**, that is, the ensemble of all the cells that must be examined to determine the state of the considered cell;
- the *evolution rules*, also called dynamic equations of the system. They are local in space and time, that is, their value depends only on the value of the state of a neighborhood of cells for a fixed number of previous time steps (usually one).

The properties of uniformity, locality and discreteness that define CA make them suitable to reproduce the behavior of complex dynamic systems, characterized by discrete elements with local (usually nonlinear) interactions. So, CA may be considered as an alternative to differential/difference equations in building and computing mathematical models of nature, as they are capable of describing systems with a great number of degrees of freedom.

3. BASIC PHYSICS OF LASER–PLASMA INTERACTIONS

In this section, we give a brief overview of the properties of a plasma and of the interactions which take place inside it. The goal is both to give some basics notions (for *nonspecialists*) regarding the physics we want to simulate, but also to give a basis for the implementation of the interaction rules (i.e., the CA evolution laws) described in the next section.

Plasma is a material in which the majority of the atoms and molecules are dissociated in positive ions and electrons. In our case, we refer to plasmas which are generated by the interaction of a short-pulse high-intensity laser with a gas. Even with such very fast lasers, a very high ionization degree is achieved during the very first phases of the interaction, after which the laser interacts with the plasma. Hence, in our physical models and in the CA code which implements them, we will neglect the physics connected to ionization of atoms and molecules in the gas which is only important at the beginning, and we will concentrate on later phases. However, it is worth noting that including ionization appears a rather easy task.

As already recalled in the introduction, the laser produces very short pulses ($\approx$100 fs) and is focused on a small focal spot ($d \approx 10\ \mu$m). The transverse dimension of such a plasma region is of the order of the focal spot size, and the longitudinal one is of the order of the lens focal depth ($L \approx 100\ \mu$m). Such small volume ($V \approx 8 \times 10^{-9}$ cm^3 or 8000 μm^3) contains a huge number of molecules ($\approx 2 \times 10^{11}$ corresponding to a density of 2.7×10^{19} molecules/cm^3) for a gas at atmospheric pressure. Evidently such numbers only allow a representation of the physical system through statis-

https://doi.org/10.1017/S0263034601194103 Published online by Cambridge University Press

tical quantities. Hence the typical parameters usually used to represent the physical state of a plasma are:

- the electron density (n_e) and the ionic density (n_i) both usually expressed in cm^{-3}. Electric charge conservation implies that $n_e = Z^* n_i$ where Z^* is the average ionization degree.
- the electron temperature (T_e) and the ion temperature (T_i) usually expressed in energy units (i.e., eV). The large mass difference between electrons and ions implies different inertia. This means that, while electrons are easily and quickly heated by the incident laser beam, ions react on a very different time scale. So, we may have $T_i = 0$ eV (or the initial, very low, gas temperature) while T_e reaches several tens electron volts. On the other end, at very late times thermal equilibrium implies $T_e = T_i$.

The propagation of a laser beam in the plasma is substantially different from that in vacuum or in an underdense gas. Indeed the dispersion relation is:

$$\nu^2 = \nu_p^2 + c^2/\lambda^2, \tag{1}$$

where c is the velocity of light, ν and λ are the laser frequency and wavelength, and ν_p is the plasma frequency (whereas in vacuum we get the usual relation between wavelength and frequency $\nu = c/\lambda$). The plasma frequency characterizes the electron motion: A plasma at equilibrium is neutral, whenever a charge separation is generated, a strong electric field arises which moves the charged particles in order to restore the initial equilibrium conditions. This produces "plasma oscillations" characterized by a proper plasma frequency.

The presence of these plasma oscillations reflects in a dependence of the index of refraction of the plasma n on the electron density

$$n(x, y, z) = (1 - n_e(x, y, z)/n_c)^{1/2} \tag{2}$$

that produces, as we will see in the following, a feedback effect is the core of the aspects we want to simulate. Here $n(x, y, z)$ and $n_e(x, y, z)$ are, respectively, the refractive index of the material and the electron density at the point (x, y, z), and n_c is the critical density, which represents the density value above which an electromagnetic wave cannot propagate in the plasma.

Moreover, typically the distribution of laser intensity is characterized by a cylindrical symmetry and by a Gaussian shape both in space and time:

$$I(r, t) = I_0 \exp[-2.77(r/r_0)^2 - 2.77(t/\tau)^2)], \tag{3}$$

where r_0 and τ are the values corresponding to $I_0/2$ in space and time (i.e., half the FWHM values). Typically, in the kind of experiments we want to simulate, we have I_0 at least of the order of 10^{17} W/cm^2 at 1 μm (near infrared radiation). The photon energy is given by Planck relation as $E = h\nu = hc/\lambda$ and is $\approx$1 eV. The total energy in the laser pulse is obtained by space and time integration of Eq. (3):

$$E_L = \int dt \int 2\pi r\, dr I(r, t) \approx 10 \text{ mJ}. \tag{4}$$

This corresponds to a number of photons in the pulse $\approx 6 \times 10^{16}$. As in the case of matter particles, we see that an individual representation of single photons is not possible and we turn to using a photon density n_{ph} (measured in cm^{-3}).

Also in the experimental setup, a lens is used to focus the laser pulse to the small focal spot with diameter $d \approx 10$ μm so to obtain the very high intensity quoted before. Usually the F number of the lens is of the order of 1/3 which means that the lens diameter is one-third of its focal length. This tight focus reflects in a short focal depth ($L \approx 100$ μm as previously quoted).

After describing the type of particles that play a role in laser–plasma interactions (electrons, ion, photons), we give a brief description of the basic interactions which take place between them. We make the further simplifying approximation of considering the positive ions as a fixed background as a consequence of their large inertia. Such assumption allows the system description to be reduced to electrons and photons. While it is generally valid in the initial stages of the interaction, this assumption may fall at later times not only in connection with the ionic timescale, but also as a consequence of the huge electric fields which can be produced by the charge separation connected to electron displacement.

1. Electron–electron interactions. Electrons interact between themselves via the Coulomb electric field. Unlike in vacuum, in a plasma, a screening effect due to the presence of the many charged particles must be taken into account. This reflects in the existence of an effective shielding distance (the Debye length).
2. Photon–electron interactions. Photons may act over the electrons by means of the *ponderomotive* forces. These are the results of radiation pressure and tend to move the electrons away from the regions where the intensity of electromagnetic field is higher. The force acting on a single electron is

$$F_p = -\nu_p^2 \nabla I/(n_e c\nu)^2, \tag{5}$$

   where I is the laser pulse intensity that can be alternatively expressed through the local instantaneous photon density.
3. Electron–photon interactions. Electrons act over the photons via the changes in the plasma local refractive index, as expressed by Eq. (2). The changes in $n(x, y, z)$ induce both changes in the photon direction (in agreement with Snell's law) and in photon velocity. In our case, the plasma has a density which is typically a factor of 100 smaller than n_c, so that the second effect

https://doi.org/10.1017/S0263034601194103 Published online by Cambridge University Press

is practically negligible. (We recall that $n_c \approx 10^{21}$ cm^{-3} for a laser wavelength ≈ 1 μm, while considering, e.g., a fully ionized hydrogen plasma produced from gas at atmospheric pressure, $n_e \approx 5.4\ 10^{19}$ molecules/cm^3.)

4. Photon–photon interactions. Obviously photons do not interact with each other. However, we must consider that, being fundamental particles, they are subject to Heisenberg's principle. In our case, this has important consequences: Passing through the lens which focuses them, their position become determined within a dimension D (the diameter of the lens). This implies an uncertainty of the order of h/D (h being Planck's constant) in the momentum of the photon along the same direction, which reflects in the spatial spread of photons in the focal plane. This is the only way of introducing the departure from geometrical optics (which would imply a perfect focusing in a geometrical point and an infinite laser intensity in the focal point) in a purely particle context, as those treated by CA codes.

Apart from these interactions it must be considered that both electrons and ions are subject to a random motion (due to thermal agitation at the temperature T) and to a hydrodynamical pressure. This last can be treated analogously to the radiation pressure. Both these effects have been neglected in the present work because, on the considered time scale, they are predicted to have a smaller influence with respect to the main interactions we have considered here (and because this is a preliminary work).

Due to the photon–electron interactions and ponderomotive forces, when an electromagnetic field propagates in plasma, electrons are forced to move from the equilibrium position to the areas where the intensity of the field is smaller. The induced variation of the electron density creates a gradient of the refractive index that modifies the photon motion in the plasma (electron–photon interaction), diverting their original direction of motion. This creates an interaction loop characterized by a feedback mechanism, as evidenced in Section 5.5 (see also Fig. 8). Due to this effect, the laser may undergo focalization (self focusing effect) in the plasma, provided the laser power is bigger than a given critical power (Amiranoff *et al.*, 1995; Lontano, 1995).

4. CELLULAR AUTOMATON IMPLEMENTATION OF LASER–PLASMA INTERACTIONS

In this section, the main features of the proposed model will be described. In the following, the practical implementation of each interaction introduced in Section 3 will be outlined. All the CA rules will be introduced on the same topological structure, that is, the cellular space. In particular, a two-dimensional (2D) triangular lattice with hexagonal symmetry has been chosen. The cellular space represents a transversal section of the region filled with the plasma where the laser–plasma interaction will take place (see Fig. 1). The laser beam is assumed to propagate initially in the z direction, and $z = 0$ is the optical axis of the system (while we call y the perpendicular direction). Due to the propagation of radiation in the plasma, the dimension of a cell l and the discrete time step t must satisfy the following condition:

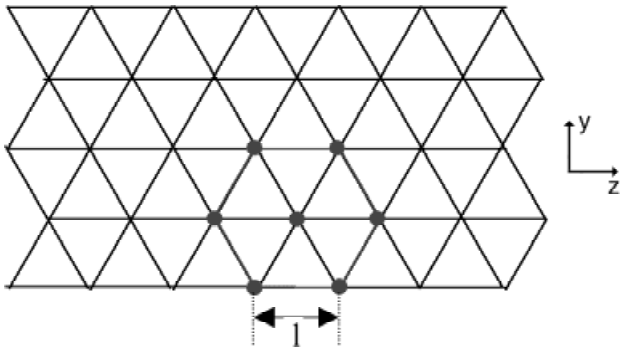

Fig. 1. Cellular space with triangular geometry and hexagonal symmetry. The CA cells are placed on the vertex of the triangles. Shown are the classical hexagonal neighborhood and the spatial size l. The horizontal axis ($z = 0$) is taken to be the optical axis of the system.

$$l/c = \Delta t, \tag{6}$$

where c is the speed of light in vacuum. The relationship (6) between the automaton spatial step l, that is, the distance between two nearest cells of the lattice, and the discrete time step Δt will be fulfilled in all the rules of evolution that will be used in this paper.

Typically, we will choose a time step $\Delta t \approx 1$ fs that implies $l \approx 0.3$ μm. These values allow a sufficient resolution both in time ($\tau/t \approx 100$) and in space ($d/l \approx 33$).

The state variables of the model depend on both time and space, that is, the cell position. In particular, the number of electrons at time k in the cell (i, j) will be denoted by $N_{el}(k)(i, j)$ and the number of photons for each direction of motion s will be indicated by $N_{sph}(k)(i, j)$. Then, the interactions described in Section 3 can be described by three different evolution rules.

Finally, we notice that the chosen topology for the cellular space is two-dimensional (although a three-dimensional (3D) model could possibly be considered in the future). By assuming translational symmetry, this is hence useful to simulate the interaction of a laser beam with a plasma slab of a given thickness t. The number of electrons in each CA cell, $N_{el}(k)(i, j)$, can be related to the electron density, $n_e(k)(i, j)$, by the obvious relation

$$N_{el}(k)(i, j) = n_e(k)(i, j)\ (3\sqrt{3}\, l^2 t/2),$$

that is, through the cell volume. The same relations holds for ion and photons.

To obtain meaningful numbers, t must be of the same order of the focal spot size. It is important to fix the cell

https://doi.org/10.1017/S0263034601194103 Published online by Cambridge University Press

thickness t because this determines the number of electrons, ions, and photons in each cell, and the absolute values of the forces depend on the number of particles (although their relative importance depends on particle densities).

In a more realistic and interesting case, our 2D CA model could be used to simulate 3D geometries with axial symmetry around the optical axis. The only difference in this case is that the volume assigned to each CA cell is that of the torus with the hexagonal cell as base, which depends on the distance from the optical axis. As a consequence, cells far from the axis will have a bigger volume and, for the same particle density, will include more particles, a factor which must be taken into account when computing the forces. (In this preliminary work, we made no attempt to simulate such axially symmetric problems.)

4.1. Photon propagation

The laser pulse can be seen as a bunch of photons coming in the region filled with the plasma from one side (say the left) and outgoing from the opposite one (say the right). Hence, in order to describe correctly the propagation of photons, the neighborhood **N** of a cell (i,j) for this evolution rule will be taken nonsymmetric. This is not strictly necessary, but leads to a computational simplification. In our CA code, we consider a realistic case of laser beam propagation. In particular, we forget the plane wave approximation, as done, for instance, in Cattaneo *et al.* (1996) and Previdi (2000), and we consider the case of a beam focused through a lens, converging down to a focal position and diverging again. Although apparently simple, this problem is difficult to be implemented with a CA. Indeed, it is necessary to settle the possible infinite directions of propagation for the photons on the cellular space, where only six directions are available, that is, NO, NE, E, SE, SO, O (see Fig. 2).

So, the neighborhood of the cell (i,j) is defined by all the cells that lie along the possible directions of motion that end in the cell (i,j), that is,

$$\mathbf{N}(i,j) = \{(i^*,j^*)\}, \text{ so that the cell } (i,j) \text{ can be reached starting from } (i^*,j^*) \text{ and moving in the NE, SE, E directions.} \tag{7}$$

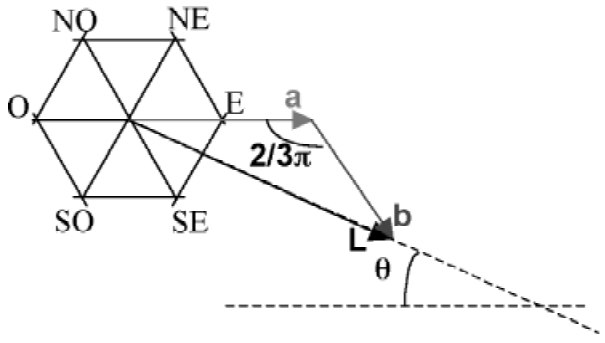

Fig. 2. Example of the decomposition of the motion of a photon.

Since it is not possible to manage an infinite number of directions, a quantization of the possible directions is performed, that is, only a finite number $s = 1,\ldots,M$ is considered. In particular, the CA spatial steps and the focal length of the focusing lens fixes the number of possible initial directions of motion. Then, each of the possible directions is decomposed along the available directions of the cellular space. As an example, consider a photon moving a distance L along a direction with angle between the E and SE directions (see Fig. 2). The following decomposition expression for the motion is obtained:

$$a(i,j) = \frac{L\cdot\sin\left(\frac{\pi}{3} - \theta(i,j)\right)}{\sin\left(\frac{2}{3}\cdot\pi\right)}$$

$$b(i,j) = \frac{L\cdot\sin(\theta(i,j))}{\sin\left(\frac{2}{3}\cdot\pi\right)}. \tag{8}$$

Then, the number of discrete space steps n_E in the E direction and n_{SE} in the SE direction is computed by

$$n_E = [a(i,j)/l] \qquad \text{and} \qquad n_{SE} = [b(i,j)/l],$$

where [ ] is the operator which takes the nearest integer of its argument.

The CA rule of evolution describing the motion of photons is the following:

$$N^{(s)}_{ph_{(k+1)}}(i,j) = \sum_{r=1}^{M} \sum_{(i^*,j^*)\in\mathbf{N}(i,j)} N^{(r)}_{ph_{(k)}}(i^*,j^*)\cdot R^{(r,s)}_{(k)}(i^*,j^*) \tag{9}$$

with

$$R^{(r,s)}_k(i^*,j^*) = \begin{cases} 1 & \text{if the destination of a photon with direction } r \text{ in the cell } (i^*,j^*) \text{ at time } k \text{ is the cell } (i,j) \text{ at time } k+1 \text{ and its final direction of motion is } s \\ 0 & \text{in all other cases.} \end{cases}$$

Equation (9) gives the number of photons in the cell (i,j) at time $k+1$ with direction of motion s as the sum of all the photons in the cell of the neighborhood with a given direction r which, moving in the cellular space, has the cell (i,j) as final destination and s as final direction of movement.

4.2. Electron–photon interaction and changes in the refractive index

The laser beam photons are travelling in a medium with variable refractive index. So, at each time step, it is necessary to evaluate the current photon direction and to change the photon state variable accordingly. It is worth stressing

https://doi.org/10.1017/S0263034601194103 Published online by Cambridge University Press

that, in the present model, this is the only situation in which a photon direction can be changed.

The refraction index modification is the consequence of the variable charge spatial distribution, due to electron movements. So, local gradients in the refractive index are obtained that modify the photon direction versor. The gradient of the refraction index $\nabla n_k(i,j)$ in each cell is computed by evaluating the local refraction index difference, that is, the difference between the refraction index in the considered cell and the one in the cells of the neighborhood. Once the local values for the refraction index have been computed, the direction of the photons in each cell are modified according to the local value of the refraction index by computing the "force" acting on the photon and modifying its direction of propagation. This is done by modifying at each time step the matrix $R_{(k)}^{(r,s)}(i^*,j^*)$, where (i^*,j^*) indicates the cells belonging to the neighborhood of the considered cell (i,j).

In practice the ray equation of geometrical optics is considered:

$$\frac{d}{ds}(n\mathbf{v}) = \nabla n.$$

This is an equation which changes the original direction of the photon versor **v** (the unit vector which gives the photon direction) according to the local gradient of index of refraction, and incorporates Snell's law for refraction.

4.3. Electron–electron and the photon–electron interaction (Coulomb and ponderomotive forces)

In these cases, there is no problem of direction of motion. In fact, the Coulomb and the ponderomotive forces, which determine the electron–electron–photon interaction, can act in all directions. So, the neighborhood **N** is the set of the six nearest neighbor cells plus the considered cell.

The main problem in modeling interactions involving electrons is that once the forces acting on a single electron are known, they determine an acceleration through Newton's law, that is, $a = F/m_e$, which produces changes in the velocity of the particles. In our model, electrons are considered as "static," in the sense that they have no velocity state variable (they could be considered as all having the same thermal velocity). Hence, the problem is how to describe the effect of forces in a CA context with static electrons. To do this, we consider that the motion of one electron will be uniformly accelerated during the time step t and hence the electron displacement will be

$$\Delta x = F(\Delta t)^2/(2m_e).$$

Since in the model computation we always obtain $x \ll$ l, that is, a displacement less than the CA spatial step, we have displaced over l a number of electrons given by $(\Delta x N_{el}(0)/l)$, where $N_{el}(0)$ is the number of electrons initially present in the cell. The evolution rule, describing the dynamics of the electron number in each cell, is given by

$$\begin{aligned} N_{el_{(k+1)}}(i,j) = {} & N_{el_{(k)}}(i,j) \\ & - \sum_{(i^*,j^*)\in \mathbf{N}(i,j)} \left[K_{1_{(k)}}^{(i^*,j^*)}(i,j) \left(\sum_{s=1}^{M} N_{ph_{(k)}}(i,j) \right.\right. \\ & \left.\left. - \sum_{s=1}^{M} N_{ph_{(k)}}(i^*,j^*) \right) \right] \\ & - \sum_{(i^*,j^*)\in \mathbf{N}(i,j)} [K_{2_{(k)}}^{(i^*,j^*)}(i,j)(N_{el_{(k)}}(i,j) - N_i)]. \end{aligned} \tag{10}$$

In the right side of Eq. (10), three terms are evident:

- $N_{el_{(k)}}(i,j)$, the number of electrons in the cell (i,j) at time k.
- $\sum_{(i^*,j^*)\in \mathbf{N}(i,j)} \left[K_{1_{(k)}}^{(i^*,j^*)}(i,j) \left(\sum_{s=1}^{M} N_{ph_{(k)}}(i,j) - \sum_{s=1}^{M} N_{ph_{(k)}}(i^*,j^*) \right) \right]$ represents the number of incoming (outgoing) electrons due to the effects of the ponderomotive force. This term is the sum of the contributions given by each cell of the neighborhood. For each contribution, the number of moved electrons is proportional to the gradient of the optical field intensity, here represented by the difference between the total photon number in the considered cell and the total photon number in the currently considered cell of the neighborhood.
- $\sum_{(i^*,j^*)\in \mathbf{N}(i,j)} [K_{2_{(k)}}^{(i^*,j^*)}(i,j)(N_{el_{(k)}}(i,j) - N_i)]$ represents the number of incoming (outgoing) electrons due to the effects of the Coulomb force. Also in this case, this is the sum of the contributions given by each cell of the neighborhood. The number of moved electrons is proportional to the net charge in the cells of the neighborhood, that is, the difference between the number of electrons and the number of ions in each cell (we notice that we neglect the self-forces due to the a net electric charge in the cell to the particles in the same cell).

Equation (10) contains two constants, namely $K_{1_{(k)}}^{(i^*,j^*)}$ and $K_{2_{(k)}}^{(i^*,j^*)}$, which can be both time-varying and space dependent. So, the number of electrons in the cell (i,j) at time $k+1$ is given by the number of electrons in the same cell at the previous time step modified by a quantity depending of the intensity of the Coulomb force and the ponderomotive force.

5. SIMULATION RESULTS

In this section, simulation results obtained using the model described in the previous section will be presented using a step-by-step approach. In fact, results on the effects of each single evolution rule of the CA will be outlined separately, in order to check at each step the physical coherency of the obtained results.

It follows from the definition of the interaction rules that the evolution algorithms conserve the number of electrons and photons. Indeed particles are only "moved" between adjacent cells and all photon absorption effects (ionization for instance) are neglected. However, we have verified num-

https://doi.org/10.1017/S0263034601194103 Published online by Cambridge University Press

ber conservation explicitly. The proposed algorithm also respects conservation laws requirements. In a real situation, the electrons are set in motion by ponderomotive forces: The energy they gain must be taken from the incoming laser beam. Hence, strictly, photon number conservation would imply that energy conservation is not really respected, even if this is a small fraction of the energy carried by the beam. However in our model, as we have noticed before, the electrons are "static," that is, they are moved between cells but do not gain any kinetic energy.

5.1. Propagation of light through a focusing lens

First of all, the propagation of photons in the absence of matter has been studied, in order to verify if the proposed law (see Eq. (9)) allows us to obtain focalization in geometric optics when the laser pulse passes through a thin lens. As already said, the pulse is Gaussian in space and time and has the following parameters: energy $E = 10$ mJ; pulse duration ≈ 100 fs; input spot size $r_0 \approx 15$ mm.

If no diffractive effect is considered (geometrical optics framework), focalization of the pulse in a single point on the focal axis must be obtained. Then, after focusing, the pulse must widen again and, in the absence of any perturbation, the starting situation should be reproduced on the opposite side of the CA. This is what has been obtained, but results of such simulations are not presented for the sake of brevity.

As a second step, similar simulations have been performed in the diffractive optics framework. In this case, we expect the progressive decrease of the transversal dimensions of the laser pulse until it arrives at the focal plane, where its transverse dimension is minimum and equal to the focal spot size. In Figure 3, the pulse is focused by a thin lens with f-number $f/D = 7$. It is worth noting that Figure 3, and many others in the following, have been drawn using a technique typical of CA. The figure represents the CA (stretched to a matrix representation) and the value of the considered state variable is plotted in gray scale, the darker corresponding to a higher value of the state variable.

The results in Figure 3 allow the laser beam size to be measured as a function of time (space). The resulting trend is shown in Figure 4, where the focal size is about 5 μm. The obtained trend can be compared with the analytical calculation for a Gaussian laser beam, which is

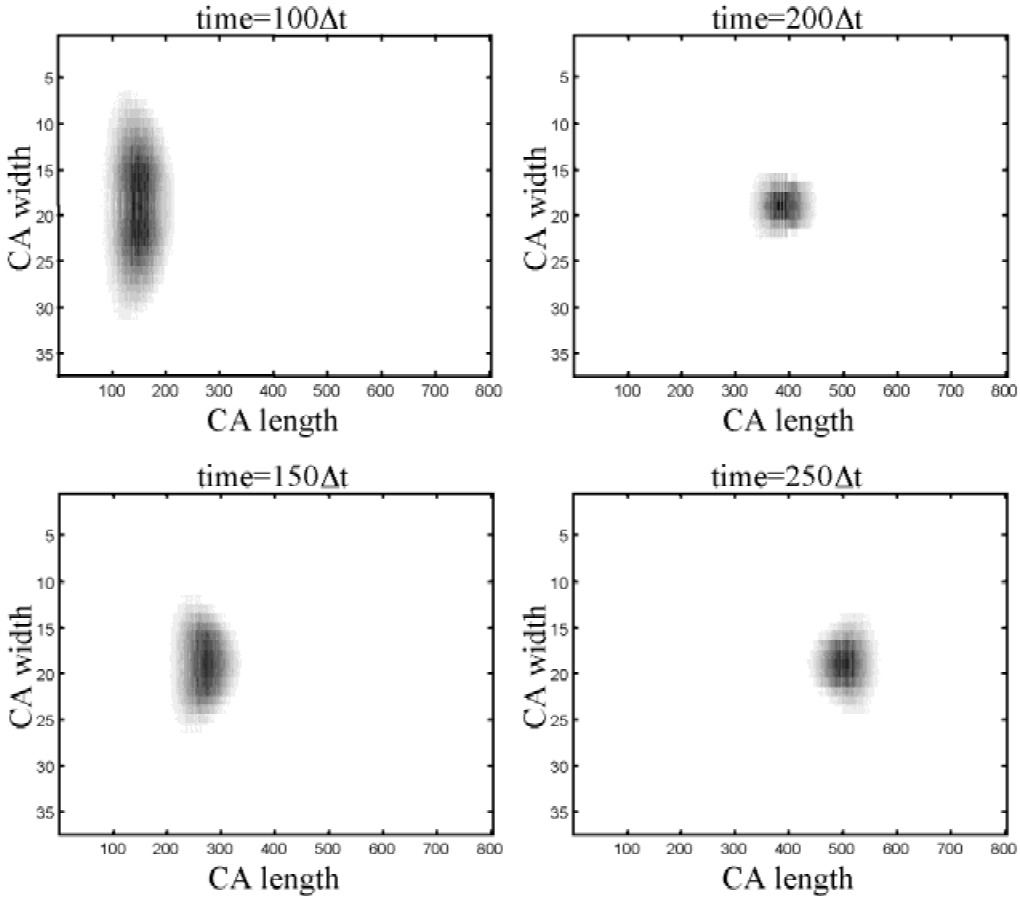

Fig. 3. The laser pulse at different times, during its propagation in a vacuum region after focalization by a thin lens. The figure is in gray scale, the darker shade corresponding to a higher number of photons. The CA spatial step is $l = 1$ micron; each simulation time step is $t = 3$ fs.

https://doi.org/10.1017/S0263034601194103 Published online by Cambridge University Press

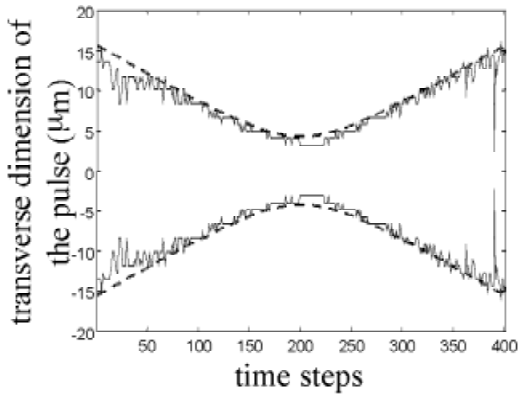

Fig. 4. Width of the laser pulse (expressed in microns, with respect to the central axis of the CA) as a function of time (solid line). Theoretical prediction from diffractive optics (dotted line).

$$R(z) = w_0\left(1 + \left(\frac{Fz}{w_0^2}\right)^2\right)^{1/2} \tag{11}$$

where $z = 0$ corresponds to the focal point; w_0 is the focal spot diameter and $F = D/f$ is the f-number of the thin lens of diameter D. As already recalled, w_0 can be obtained by application of the Heisenberg principle, by noting that $w_0 = f\Theta$ (where Θ is the beam divergence, i.e., the angle under which the focal spot is seen by the lens), which is given by $\Theta = \Delta p/p = (h/D)/(h\nu/c) = \lambda/D$.

Hence the photons (initially assumed to propagate parallel to the optical axis) acquire a momentum component in the y direction Δp when they go through the lens of aperture D. In our model the lens corresponds to the left boundary of the CA space. The photons are then injected with a momentum component p_y which is randomly distributed with a zero average and a width given by Δp written above. Hence the only nonlocal information which is necessary to reproduce the diffractive optics behavior shown in Figure 3 is that the presence of the lens fixes the photon position within an incertitude equal to the lens diameter D.

Numerical results in Figure 3 compare very well with analytical predictions concerning both the focal spot size and the focal depth, that is, the distance over which the variation in intensity is less than 10% of the maximum value achieved at the focus.

5.2. Effect of ponderomotive forces

In this section, the effects of ponderomotive forces are introduced. In particular, it is supposed that these are the only forces acting on the electrons, that is, no Coulombian interaction is active. This is equivalent to considering as a rule of evolution only the first two terms on the right-hand side of Eq. (10). So, electrons are forced to move away from their initial position towards regions where the intensity of the optical field is smaller.

Figure 5 shows temporal evolution of the system state variables (photon number and electron number). After the passage of the laser pulse, a lower electron density plasma channel is obtained. Figure 6 shows the obtained transversal modulation of electron density after the propagation of the beam in the region.

5.3. Beam propagation in a medium with a constant refractive index

The passage of a laser pulse in a plasma causes the formation of a central channel with lower electron density, due to ponderomotive forces which move the electrons towards regions with smaller optical intensity. So, the electron density is no longer uniform in the region filled with the plasma. Consequently, the refractive index is not uniform in that region too. In particular, if the Coulomb interaction is switched off, so as to say that in Eq. (10) the third term on the right-hand side is zero, no other change in the electron density and in the refractive index will occur (since we have neglected hydrostatic pressure and thermal motion). Now, consider this "frozen time" situation and send into this region a second laser pulse. As a first approximation, it can be supposed that the refractive index of the region has a parabolic profile and so, the second laser pulse will travel through a region with constant (in time) refractive index due to a constant electron distribution. The algorithm which is used to take refraction into account is described in Section 4.2.

In simulations, photons are introduced in the CA from the left side as rays of light with different incident angles. Rays have been simulated by using photon number profiles very narrow in space and with indefinite duration in time. Results of simulations are qualitatively and quantitatively similar to those obtained using ray-optics theory. In Figure 7, the propagation of rays through the region is shown for different incident angles.

Finally, it is worth noting that the propagation of photons in this plasma channel is exactly analogous to that in an optical fiber (in both cases the refractive index is higher on the central longitudinal axis) and the same theory and analytical formulas do apply (Gowar, 1984).

5.4. Effects of Coulomb forces

When the radiation has completely crossed the region filled with plasma, an inhomogeneous distribution of charge is obtained (a transversal section can be seen in Fig. 6). So, an electric field will recall the electrons (positive ions are still considered fixed) towards their equilibrium positions. Relaxation of electrons from the perturbed situation generated in Section 5.2 is obtained by effect of the electrical field generated by the charge spatial distribution. Plots of simulations are omitted for the sake of brevity. The physical parameters used are the same as in the simulation in Section 5.2. The final effect is simply a relaxation of the electron number in each cell to the initial value (here $N_{el_{(0)}}(i,j) = 8 \times 10^7$). Only the simulation time step is different: Here $t = 1$ ps. So, the process is slower than the depletion phenomenon caused by the laser pulse.

https://doi.org/10.1017/S0263034601194103 Published online by Cambridge University Press

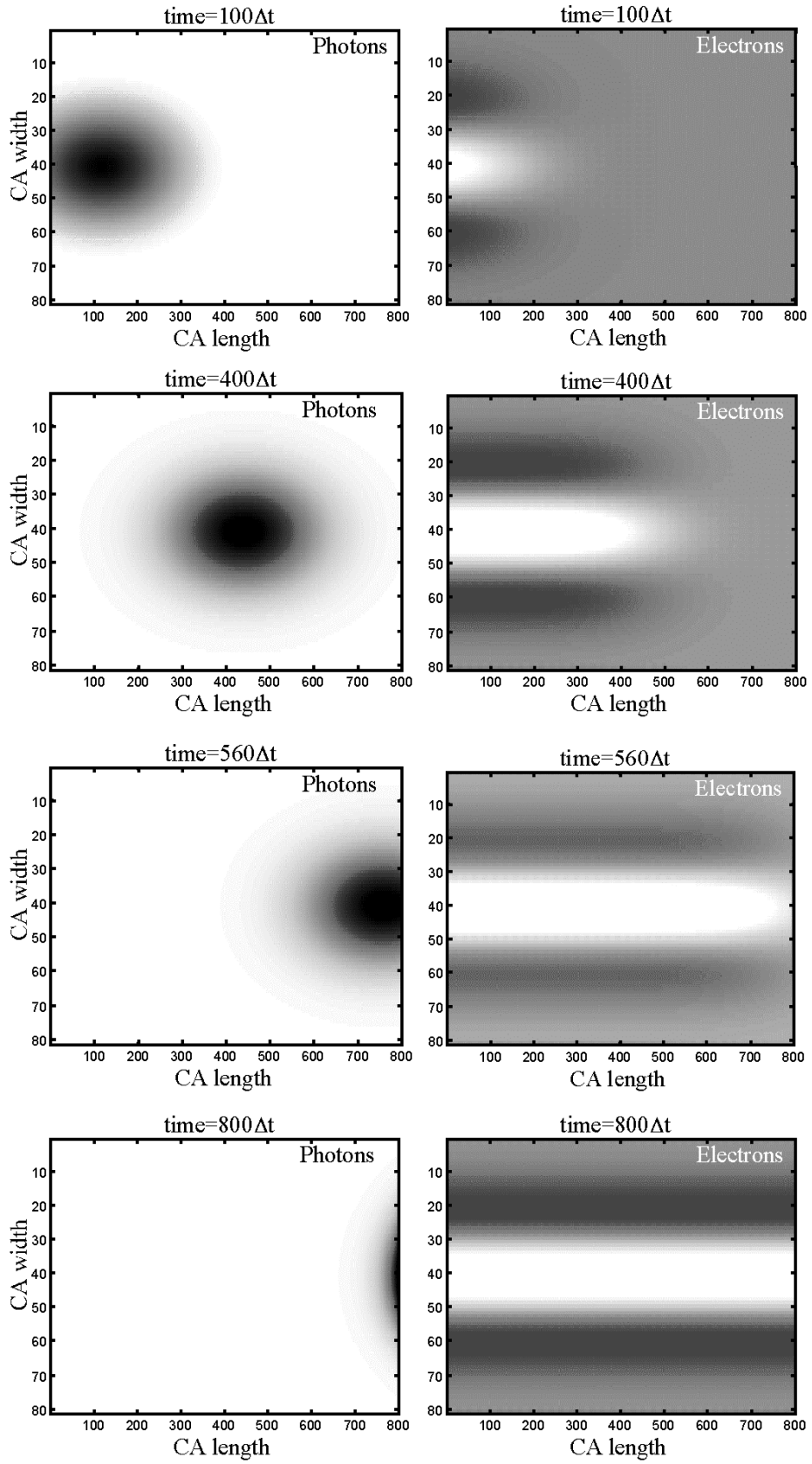

Fig. 5. Photon number and electron number in gray scale (the darker, the higher the number) at different stages of time evolution of the simulation. The laser pulse propagates with a direction parallel to the optical axis pushing the electrons in regions where the intensity of the field is smaller. Since only ponderomotive force is considered and the refractive index of the medium is considered constant (i.e., the electron–photon interaction has been switched off in this simulation), no reaction due to charge displacement is visible.

https://doi.org/10.1017/S0263034601194103 Published online by Cambridge University Press

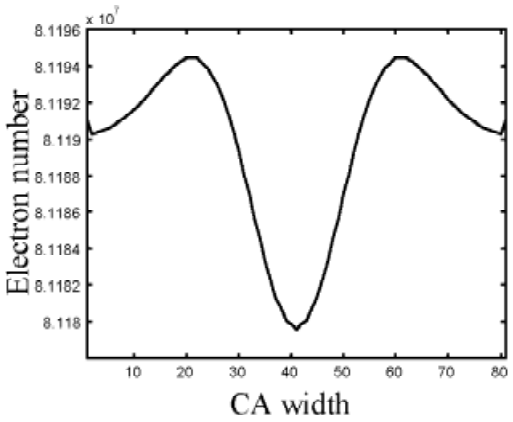

Fig. 6. Electron number on a transversal section of the plasma region after the passage of a laser pulse, considering only the effects of ponderomotive forces. The following physical parameters have been used in the simulation: $l = 0.25$ μm; $t = 0.834$ fs; refractive index $n = 1$; $r_0 = 5$ μm; $N_{el_{(0)}}(i,j) = 8 \times 10^7$ for all i,j. The pulse has been chosen with a peak amplitude of 9×10^{12} photons.

5.5. Coupled effects of ponderomotive force and refraction index changes: Self-focusing

Finally, the rules of evolution of all the interactions are simultaneously considered. The coupled effects of ponderomotive force on electron distribution, the consequent modification of the refractive index and its effects on the optical propagation are described in Figure 8, where a clear feedback is evident in the process dynamics.

When an electromagnetic wave propagates in a hot plasma, electrons are forced to move towards regions where the intensity of the optical field is smaller, because of ponderomotive force. The obtained charge density gradient causes a Coulombian recall field that moves electrons in the opposite direction (positive ions will still be considered fixed). The

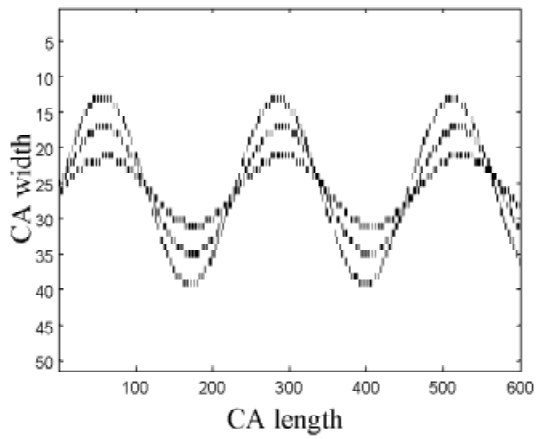

Fig. 7. Propagation of light rays in a plasma channel produced by ponderomotive forces. The refractive index profile is assumed to be parabolic with maximum refraction index $n_M = 1.55$; bulk refraction index $n_b = 1.4$; the time step used in the simulation is $t = 10$ fs.

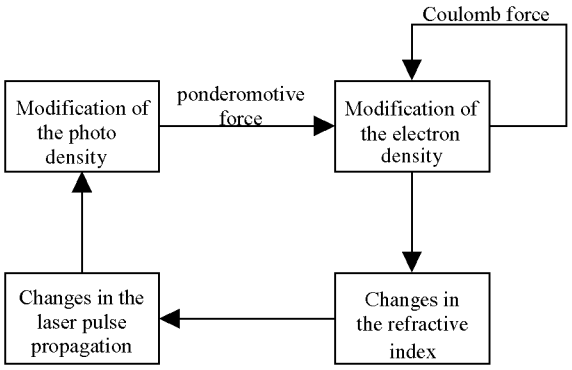

Fig. 8. Schematic of laser–plasma interactions.

local and instantaneous variation of the electric field causes a gradient of the refractive index, which influences the photon motion in plasma. The final effect of this process is different depending on the power of the incoming laser pulse. In particular, if the power is sufficiently high (i.e., higher than the so called "critical power" which can be calculated from well-known formulas (Amiranoff *et al.*, 1995)) the modification of the refraction index is so that the laser pulse is focused in the material.

By considering all the interactions, simulations are provided showing the arising of self-focusing effects. In particular, Figure 9a shows the propagation of a laser pulse with power below the critical one. Figure 9b shows the self-focusing effect. The plots are obtained as a three level plot of the photon number at different times.

6. DISCUSSION AND CONCLUSIONS

As it is evident from the approach used in the presentation, the present work should be considered only as a preliminary one. However, this paper already shows the potential, as well as the main limits, of the CA approach to the simulation of laser–plasma interactions.

A first advantage of CA models is the insight they may give in the complex physical phenomena that are going on during the interactions. In the framework of CA models, the macroscopic physical effects simply arise from the "replication" of simple local and microscopic physical laws. In particular, first, we have obtained interesting results, both qualitatively and quantitatively, concerning the propagation and focusing of the laser beam in free space and in a frozen density profile. This last point may be of interest also for the simulation of laser beam propagation in optical fibers. Secondly, we have successfully described the creation of a plasma channel due to ponderomotive forces. Results on relaxation of the plasma channel and on self-focusing (again due to ponderomotive forces) of the laser beam in the plasma are instead at the moment only qualitative.

There are some limits connected either to our specific CA model or to CA in general. In the presented model, we consider the electrons as "static," that is, they may move

https://doi.org/10.1017/S0263034601194103 Published online by Cambridge University Press

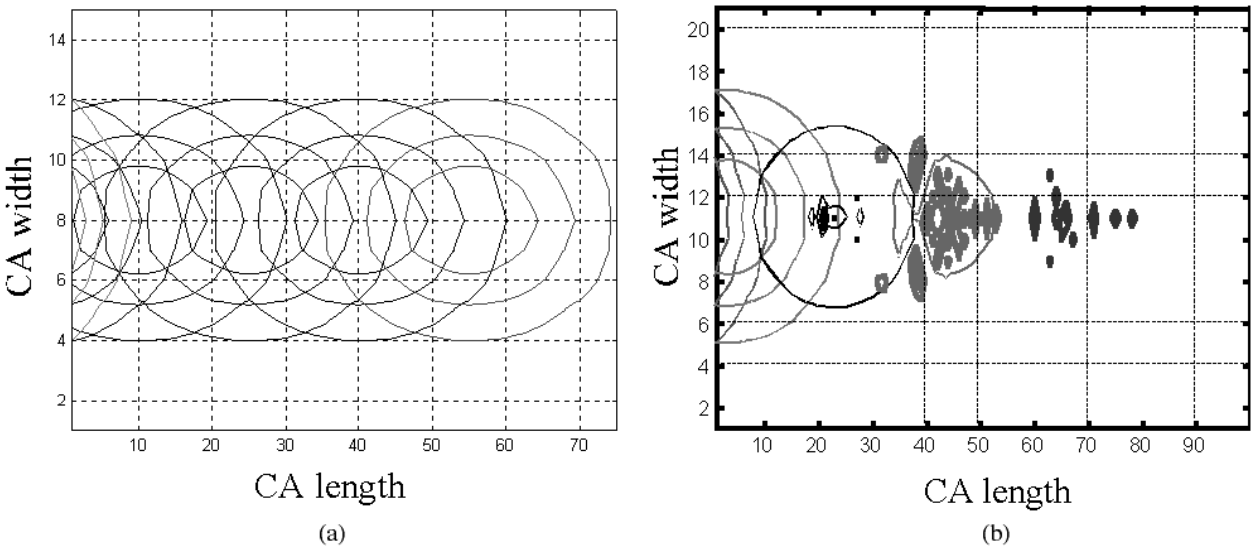

Fig. 9. Three-level plots of the pulse during its propagation in the plasma taken every 20 time steps (56 fs). The chosen level are 30%, 60%, and 90% of the peak number of photons. The physical parameters of the incoming pulse are $\tau = 100$ fs and $r_0 = 5$ μm. The initial electron density in the plasma $N_{el_{(0)}}(i, j)$ for all i, j corresponds to a critical power $P_{cr} = 33$ GW. The laser pulse energy is fixed so that the ratio between the power of the laser pulse and the critical power is 0.33 in the first case (a) and 3 in the second (b).

from one cell to another but they are not characterized by a velocity. Hence, we cannot describe even simple phenomena such as plasma oscillations which are based on the transformation of (electric) potential energy in kinetic energy and vice versa. As a consequence, we are not able to describe also more complex phenomena, such as: the acceleration of electrons in the laser beam wake-field; the creation of electron currents and of the magnetic fields they produce (which may induce a pinching effect in the plasma); and the variation of electron mass with velocity in the relativistic interaction regime. Since this last phenomenon is the origin of relativistic self-focusing, it follows that it cannot be modeled with our CA model (here we only modeled ponderomotive self-focusing).

Introducing the electron velocity in this CA code is, in principle, easy: It is sufficient to introduce many electron families, each characterized by its own velocity, in a similar way to what we have done with photon directions. However, in practice, this greatly increases the model complexity. In fact, the range of the electron velocity in the physical system is very large. The electron speed ranges from electron thermal velocity to (almost) light speed, for the electrons accelerated by the laser beams. Also, the thermal "slow" electrons and the "fast" ones have very different time constants and each of them must be dealt with sufficient resolution. On the other side, there are phenomena that are intrinsically difficult to simulate with CA models, which are intrinsically "particle-based" codes. Indeed, in this context, the laser beam is described as a bunch of photons and it is difficult to consider the "wave-based" properties of an electromagnetic field. As a consequence, the generation of the electromagnetic fields (and even of magnetostatic fields connected to electron currents) is difficult to be described, as well as all long-range forces arising in the plasma as a consequence of the plasma dynamics itself. We recall again that in plasmas, this is not the case of electrostatic (Coulomb) forces that are effectively screened over a distance of the order of the plasma Debye length. Hence, Coulomb forces in plasma are strictly short range (local), and this makes their modeling easy to obtain in a CA context.

The previous considerations fix an optimal range of laser and plasma parameters for which CA simulation of laser–plasma interactions can be performed and give physically sensible results. This is the regime of short pulse lasers at intermediate intensity (high, but nonrelativistic) and moderate plasma density. This range is dominated by the effects of ponderomotive forces, while phenomena like electron acceleration and relativistic effects can reasonably be neglected. Finally, one main advantage of this modeling approach is the computation time: The presented CA model has been simulated with very short computational times on single processor sequential (PC) computers. In fact, CA lend themselves naturally for parallel computer implementation, realizing a direct correspondence between the model structure (i.e., the cellular space topology) and the computation tool (i.e., the displacement of the processors in the machine). As an extreme consequence, it could be thought a direct one-to-one correspondence between the automaton cells and the computer processors.

ACKNOWLEDGMENTS

This research was supported by MURST Project "Identification and Control of Industrial Systems." We also acknowledge the support of the FEMTO Programme of the European Science Foundation.

https://doi.org/10.1017/S0263034601194103 Published online by Cambridge University Press

REFERENCES

Amiranoff F., Malka, V. & Batani, D. (1995). In *Non Linear Dynamics* (Costato, M., and Degasperis, A., Eds.), Bologna, Italy: Editrice Compositori. pp. 119–126.

Atzeni, S. (1995). *Jpn. J. Appl. Phys.* **34**, 1980.

Batani, D., Davies, J., Bernardinello, A., Hall, T.A., Koenig, M., Pisani, F., Djaoui, A., Norreys, P., Neely, D. & Rose, S. (2000). *Phys. Rev. E* **61**, 5725.

Bennet, C.H., Toffoli, T. & Wolfram, S. (1986). *Cellular Automata 1986 Conference*. Cambridge, MA: M.I.T. Press.

Bernardinello, A., Batani, D., Masella, V., Koenig, M., Benuzzi, A., Krishnan, J., Pisani, F., Djaoui, A., Norreys, P., Neely, D., Rose, S., Hall, T.A., Ellwi, S. & Fews, P. (1999). *Laser Part. Beams* **17**, 529.

Bruschi M., Santini, P.M. & Ragnisco, O. (1992). *Phys. Lett. A* **51**, 169.

Burks, C. & Farmer, D. (1984). *Physica D* **10**, 157.

Cattaneo, G., Milani, M., Magni, F. & Rigotti, M. (1996). *Il Nuovo Cimento B* **111**, 863.

Chen, S., Doolen, G. & Lee, Y.C. (1988a) *Complex Systems* **2**, 259.

Chen, H., Matthaeus, W.H. & Klein, L.W. (1988b). *Phys. Fluids* **31**, 1439.

Dab, D. & Boon, J.P. (1990). In *Proc. Int. Winter Workshop*, (Manneville, P., Boccara, N., Vichniac, G.Y. and Bidaux, R., Eds.). New York: Springer-Verlag.

Dalla, S. & Lontano, M. (1995). In *Non linear dynamics*, (Costato, M. and Degasperis, A., Eds.), pp. 211–218. Bologna, Italy: Editrice Compositori.

Davies, J., Bell, A., Haines, M. & Guerin, S. (1997). *Phys. Rev. E* **56**, 7193.

Di Gregorio, S., Rongo, R., Spataro, W., Spezzano, G. & Talia, D. (1996). *IEEE Comp. Sci. Eng.* **3**, 33.

Doolen, G.D. (1991). In *Proc. NATO Advanced Research Workshop*, (Doolen, G.D., Ed.), Amsterdam: North-Holland.

Frish, U., Hasslacher, B. & Pomeau, Y. (1986). *Phys. Rev. Lett.* **56**, 1500.

Gremillet, L., Amiranoff, F., Baton, S., Gauthier, J.C., Koenig, M., Martinolli, E., Pisani, F., Bonnaud, G., Lebourg, C., Rousseaux, C., Toupin, C., Antonicci, A., Batani, D., Bernardinello, A., Hall, T., Scott, T., Norreys, P., Bandulet, H. & Pepin, H. (1999). *Phys. Rev. Lett.* **83**, 5015.

Gowar, J. (1984). *Optical Communication Systems*, London: Prentice Hall.

Hall, T., Ellwi, S., Batani, D., Bernardinello, A., Masella, V., Koenig, M., Benuzzi, A., Krishnan, J., Pisani, F., Djaoui, A., Norreys, P., Neely, D., Rose, S., Key, M. & Fews, P. (1998). *Phys. Rev. Lett.* **81**, 1003.

Key, M. (1999). Studies of the relativistic electron source and related phenomena in petawatt laser matter interactions, Report N. UCRL-JC-135477REV1, December. Livermore, CA: Lawrence Livermore National Laboratory.

Lontano, M. (1995). In *Non linear dynamics*, (Costato, M. and Degasperis, A., Eds.), pp. 237–242. Bologna, Italy: Editrice Compositori.

Macchi, A., Califano, F., Cornolti, F., Zambon, B. & Ruhl, H. (1998). In *Science and Supercomputing at CINECA–Report '97*, pp. 522–529. Bologna Italy: CINECA.

Modena, A., Najmudin, Z., Dangor, A.E., Clayton, C.E., Marsh, K.A., Joshi, C., Malka, V., Darrow, C.B., Danson, C., Neely, D. & Walsh, F.N. (1995). *Nature* **377**, 606–608.

Mourou, G., Barty, C. & Perry, M. (1998, January). *Phys. Today*, 22–28.

Nisoli, M., Stagira, S., De Silvestri, S., Svelto, O., Sartania, S., Cheng, Z., Lenzer, M., Spielmann, C. & Krauss, F. (1998). In *Superstrong Fields in Plasmas* (Lontano, M., Mourou, G. & Pegoraro, F., Eds.), pp. 304–313. AIP Conf. Proc. 426, Woodbury, CT: American Institute of Physics.

Packard, N. (1985). In *Proc. 1st Int. Symp. Science on Form*, Tsukuba, Japan.

Pisani, F., Antonicci, A., Bernardinello, A., Batani, D., Martinolli, E., Koenig, M., Gremillet, L., Amiranoff, F., Baton, S., Hall, T., Scott, D., Norreys, P., Djaoui, A., Rousseaux, C., Fews, P., Bandulet, H. & Pepin, H. (2000). *Phys. Rev. E* **62**, R5927.

Previdi, F. (2000). In *Proc. MTNS2000*, Perpignan, France.

Previdi, F. & Milani, M. (1998). *Il Nuovo Cimento D* **20**, 1625.

Pukhov, A. & Meyer-ter-Vehn, J. (1998). In *Superstrong Fields in Plasmas* (Lontano, M., Mourou, G., and Pegoraro, F., Eds.), pp. 93–102. AIP Conf. Proc. 426, Woodbury, CT: American Institute of Physics.

Ruhl, H., Cornolti, F., Califano, F. & Macchi, A. (1998). In *Superstrong Fields in Plasmas*, (Lontano, M., Mourou, G. and Pegoraro, F., Eds.), pp. 282–287. AIP Conf. Proc. 426, Woodbury, CT: American Institute of Physics.

Smith, S.A., Watt, R.C. & Hameroff, S.R. (1984). *Physica D* **10**, 168.

Spezzano, G. & Talia, D. (1998). In *Future Generation Computer Systems*, Vol. 13, pp. 291–302, Amsterdam: North-Holland.

Tabak, M., Hammer, J., Glinsky, M.E., Kruer, W.L., Wilks, S.C., Woodworth, J., Campbell, M.E., Perry, M.D. & Mason, R.J. (1994). *Phys. Plasmas* **1**, 1626.

Toffoli, T. (1984). In *Proc. Interdisciplinary Workshop*, (Farmer, D., Toffoli, T. and Wolfram, S., Eds.), Amsterdam: North-Holland Physics Publishing.

Wolfram, S. (1983). *Rev. Mod. Phys.*, **55**, 601.

Zepf M., Pretzler, G., Andiel, U., Chambers, D., Dangor, A., Norreys, P., Wark, J., Watts, I. & Tsakiris, G. (1998a). In *Superstrong fields in plasmas*, (Lontano, M., Mourou, G., and Pegoraro, F., Eds.), pp. 264–269. AIP Conf. Proc. 426, Woodbury, CT: American Institute of Physics.

Zepf, M., Zhang, J., Chambers, D., Dangor, A., MacPhee, A., Lin, J., Wolfrum, E., Nilsen, J., Barbee, T., Danson, C., Key, M., Lewis, C., Neely, D., Norreys, P., Preston, S., O'Rourke, R., Pert, G., Smith, R., Tallents, G., Watts, I. & Wark, J. (1998b). In *Superstrong Fields in Plasmas*, (Lontano, M., Mourou, G. and Pegoraro, F., Eds.), pp. 499–508. AIP Conf. Proc. 426, Woodbury, CT: American Institute of Physics.

https://doi.org/10.1017/S0263034601194103 Published online by Cambridge University Press